HELICOPTER VIBRATION REDUCTION WITH TRAILING EDGE FLAPS

Judah Milgram* Inderjit Chopra †

Center for Rotorcraft Education and Research
Department of Aerospace Engineering
University of Maryland
College Park, Maryland 20742

Main rotor blades with plain trailing edge flaps are investigated as a potential means of vibration reduction using a comprehensive rotorcraft analysis. The analysis is modified to incorporate an unsteady aerodynamic model including flap effects. Predicted blade and pitch link loads show adequate correlation with experimental data. An initial open loop study shows that, for a typical articulated four bladed rotor, significant reductions in fixed system 4/rev vertical shears and hub moments are possible with open loop flap deflections at 3/rev and 4/rev. The reductions are most closely associated with changes in the response of the blade third flatwise bending mode and torsional deflections. A reduction in blade torsional stiffness reduced the effectiveness of the flap in reducing vibration.

Notation

C_T	Thrust coefficient
C_L	Profile lift coefficient
$C_{L_{\mathrm{qs}}}$	Quasisteady value of C_L
M_β	Trailing edge flap hinge moment coefficient
M_Y	Blade sectional flapwise bending moment, positive for upwards blade tip deflections.
$\mathbf{L}$	Vector of sectional aerodynamic loads, $\{P\ M_\alpha\ M_\beta\}^T$
$\mathbf{x}$	Vector of local blade deflections, $\{v\ w\ \phi\}^T$
R	Rotor radius
S	Non-dimensional time, $dS = (V(t)/b)dt$
U_T	Local velocity parallel to blade undeformed axis, normalized to ΩR
U_P	Local velocity perpendicular to blade undeformed axis, normalized to ΩR, positive is velocity from above.
b	Blade section semi-chord
c_{d_0}	Sectional drag coefficient
c_f	Flap chord ratio
$\dot{h}, \ddot{h}$	Vertical velocity and acceleration of blade section
r	Radial station
α	Airfoil angle of attack
α_s	Rotor shaft angle of attack, positive for forward shaft tilt.
β	Trailing edge flap deflection, positive for trailing edge down. Also, Prandlt-Glauert compressibility correction factor, $\sqrt{1-M^2}$
λ	Local rotor inflow
μ	Advance ratio
ν_θ	Blade first torsional natural frequency
ϕ_w	Wagner's indicial lift response function
σ	Rotor solidity
θ_0	Collective pitch
$\theta_{1\mathrm{C}}$	Lateral cyclic control, positive for left cyclic
$\theta_{1\mathrm{S}}$	Longitudinal cyclic, positive for forward cyclic

*Rotorcraft Fellow; Member AHS
†Professor; Fellow AIAA

Presented at the 36th AIAA/ASME/ASCE/AHS/ASC Structures, Structural Dynamics, and Materials Conference, April 10-12, 1995, New Orleans, LA.

Introduction

In the course of early rotorcraft development the feathering blade controlled by a swashplate emerged as the favored form of rotor control. The swashplate provides a mechanically simple means of providing a 1/rev input to the blades; this is precisely what is required to meet the basic need to control the rotor thrust vector.

Subsequently, the recognition that fixed system vibration arises primarily as a result of the aerodynamic environment at the rotor disk and blade motion at higher rotor harmonics led naturally to the concept of higher harmonic (mutlicyclic) control. A review of early HHC work may be found in Ref. 1. HHC systems typically apply their higher harmonic input through the swashplate. For $N_b > 3$, this arrangement has the limitation of being unable to control the pitch of the blades independently. The need to actuate the swashplate at rotor harmonics also results in additional hydraulic systems and associated weight and maintainability penalties. HHC research has therefore led to interest in alternate means for blade control, such as jet flaps[2, 3], circulation control[4], servo flaps[5], and plain trailing edge flaps[6]. Rotor blade flaps may be further categorized by actuation means, i.e. conventional (mechanical or servoelectric) or smart structure actuation[7, 8]. Common to all these systems is the ability to control the blades independently of one another, hence the term Individual Blade Control (IBC). Note that while some writers have taken "IBC" to denote primarily those systems in which the control input is blade pitch, here it is taken in the more general sense as indicating any system capable of applying control inputs to individual blades. Note that IBC does not necessarily imply HHC. HHC systems are fundamentally frequency domain systems in that an actuator is driven at multiples of the blade passage frequency based on the harmonic content of the the vibration or hub loads. IBC systems offer greater flexibility than conventional swashplate based HHC systems in that in addition to providing a means for generic harmonic control inputs, various time domain control functions may be implemented. For example, Ham[9] has proposed a simple time domain IBC system in which the control input is based on a simple feedback system based on the estimated amplitude of the first elastic flapping mode. Other fundamentally time-domain applications of IBC would include gust load alleviation and stall flutter suppression[6, 10].

The goal of the present research is to examine the possibilities for vibration reduction with Individual Blade Control with plain trailing edge flaps. In addition to the other advantages offered by IBC systems, trailing edge flaps offer the possibility for actuation through induced strain smart actuators such as piezoceramic elements. Such actuators are mechanically simple, eliminating the need for a hydraulic slipring, and have the high bandwidth required for use with HHC and/or time domain control systems. Potential advantages of a plain trailing edge flap over a servoflap include reduced power losses due to aerodynamic drag and lower actuation power requirements.

Vibration reduction with trailing edge flaps has been the subject of several experimental and analytical studies in recent years. Spangler and Hall[11] conducted a feasibility study of induced strain activated trailing edge flaps for vibration reduction. An analytic study was performed and a piezoelectric actuator was successfully demonstrated on a non-rotating section in a wind tunnel test. Further investigations into induced strain actuated trailing edge flaps were performed by Samak and Chopra[12], Fenn *et al*[13], and Walz and Chopra[14]. Reference 12 discusses a hover stand test of a Froude-scaled model rotor with induced strain actuated trailing edge flaps. In Ref. 14 an improved bimorph piezoelectric bimorph actuator was designed and tested. Reference 13 discusses a magnetorestrictive actuator for trailing edge flaps. Recently, Ben-Zeev and Chopra[7] identified and demonstrated additional design improvements to the bimorph actuated trailing edge flap.

These studies involved plain trailing edge flaps. Such flaps are essentially hinged portions of the conventional blade and are used for lift control. Another type of flap, the servo flap, was the subject of an analytical study conducted by Millott and Friedmann[15, 16, 17]. Servo flaps are mounted aft of the blade trailing edge, and thus provide substantial pitching moments as well as changing airfoil lift characteristics. Ref. 15 described a feasibility study utilizing a spring-restrained offset-hinged rigid blade model. It was concluded that partial-span servo flaps could be just as effective as "conventional" HHC systems in which the pitch of the entire blade was varied, with the advantage of reduced power requirements. In Ref. 16, the analysis was improved to include an elastic blade model, refinements to the aerodynamic model, and parametric studies involving flap size and radial location. The investigation was extended in Ref. 17 to include a time domain solution. In all these studies a modified quasisteady version of Greenberg's aerodynamic theory was used. The flap was assumed to be driven at a number of discrete harmonics determined by a discrete time

controller updating no more than once per revolution. This is essentially a servo flap implementation of a conventional HHC scheme (see, for example, Ref. 1). The updates were made based on harmonic content of the rotating system hub loads.

In the present study a trailing edge flap in the form of a plain flap is considered. The goals of the present investigation are:

1. Develop a comprehensive rotor aeroelastic analysis capable of modeling an elastic blade rotor with plain trailing edge flap.

2. Validate the analysis with available experimental data for a conventional blade and identify important refinements to the analysis.

3. Examine the behavior of the system when operated in an open-loop HHC mode.

Analytic Model

Aerodynamics

The present investigation is based on an advanced comprehensive rotorcraft analysis[18], modified extensively to allow modelling of quasisteady and unsteady aerodynamics of flapped airfoils sections.

The aerodynamic model of Leishman[19] has been used with the unsteady terms calculated via recursively computed lift deficiency functions[20]. In the present analysis, the incompressible unsteady forces are used together with the Prandtl-Glauert compressibility correction. A full implementation of the Ref. 19 analysis is underway which will include a treatment of the compressible noncirculatory terms arising from flap deflection.

The lift on a two dimensional airfoil with plain trailing edge flap is given as

$$\begin{aligned} C_L(t) &= \frac{\pi b}{V^2}(\ddot{h} + V\dot{\alpha} - ba\ddot{\alpha}) \\ &+ \frac{b}{V^2}(-VF_4\dot{\delta} - bF_1\ddot{\delta}) \\ &+ C(k)C_{L_{\rm qs}}(t) \end{aligned} \tag{1}$$

with the F_i being functions of the flap chord ratio and

$$C_{L_{\rm qs}} = \frac{2\pi}{\beta}\left(\alpha_{\rm qs}(t) + \delta_{\rm qs}(t)\right) \tag{2a}$$

$$\alpha_{\rm qs} = \frac{\dot{h}}{V} + \alpha + b\left(\frac{1}{2} - a\right)\frac{\dot{\alpha}}{V} \tag{2b}$$

$$\delta_{\rm qs} = \frac{F_{10}\delta}{\pi} + \frac{bF_{11}\dot{\delta}}{2\pi V} \tag{2c}$$

For arbitrary airfoil motion the lift may be written in the time domain using Duhamel's superposition integral and Wagner's function as

$$\begin{aligned} C_L(t) &= \frac{\pi b}{V^2}(\ddot{h} + V\dot{\alpha} - ba\ddot{\alpha}) \\ &+ \frac{b}{V}(-VF_4\dot{\delta} - bF_1\ddot{\delta}) \\ &+ \int_{-\infty}^{S}\phi_w(S-\sigma)\frac{d}{d\sigma}C_{L_{\rm qs}}d\sigma \end{aligned} \tag{3}$$

Wagner's function may be approximated as

$$\phi_w = 1 - \sum_{i=1}^{N} A_i \exp(-b_i S) \tag{4}$$

the coefficients A_i and b_i being determined based on an exponential curve fit. The b_i are further factored by $\beta^2 = 1 - M^2$ as suggested in Ref. 19. Equation 4 together with the approximation in Equation 4 leads to the following expression for the circulatory part of the sectional airloads:

$$C_{Lc}(t) \approx C_{L_{\rm qs}}(t) - \sum_{i=1}^{N} X_i(t) \tag{5}$$

with the lift deficiency functions X_i given as functions of nondimensional time S by

$$X_i(S) = A_i \int_{-\infty}^{S} \exp\left(-\beta^2 b_i(S-\sigma)\right)\frac{d}{ds}C_{L_{\rm qs}}d\sigma$$

It can be shown (Ref. 20) that the following recursive relationship may be applied to the lift deficiency functions at discrete time points:

$$\begin{aligned} X_i(S+\Delta S) &\approx \exp(-b_i\Delta S)X_i(S) \\ &+ A_i\Delta C_{L_{\rm qs}}\exp(-b_i\Delta S/2) \end{aligned} \tag{6}$$

Here $\Delta C_{L_{\rm qs}} = C_{L_{\rm qs}}(S+\Delta S) - C_{L_{\rm qs}}(S)$. For implementation, the lift deficiency functions are computed and stored at each of the Gaussian integration points used for the spatial integration of the blade elemental matrices. The X_i are initially set to zero. Integration of the finite element in time (FET) matrices proceeds element by element at successively increasing values of azimuth and the X_i are updated using Equation (6). The final values of the X_i following integration of all the time elemental matrices are used as the starting values in the next FET iteration. A simple convergence criterion is applied based on a comparison of the initial and final values of the X_i.

The sectional lift (Equation 5) and profile drag are parallel and perpendicular to the local resultant flow and are resolved to the undeformed blade axis system by a rotation transformation through an angle $\alpha_i \approx U_T/U_P$.

Equations of Motion

The blade equations of motion are written using a spatial finite element discretization and subsequent reduction to modal space. The structural contributions to the elemental matrices are described in Ref. 18. The aerodynamic contributions to the elemental mass, stiffness, and damping matrices as well as the force vector are derived from Equation 5 using a virtual work approach. The closed-form expressions for the sectional blade loads L, D, and M_α are be written in terms of local blade velocities U_T and U_P which in turn related to the local blade deflections u, v, v', w, w', and ϕ:

$$\begin{aligned} U_T &= x + \mu(\sin\psi + v'\cos\psi) + u + \dot{v} \\ U_P &= \lambda + \mu w'\cos\psi + \dot{w} \end{aligned}$$

The virtual work for the spatial element is

$$\delta W = \int_{\text{element}} \delta\mathbf{x}^T \left\{ \begin{array}{c} L \\ D \\ M_\alpha \end{array} \right\}$$

Introducing a spatial shape function matrix $\mathbf{H}$ such that $\mathbf{x} = \mathbf{Hq}$ leads to

$$\delta W = \int_{\text{element}} \delta\mathbf{q}^T\mathbf{H}^T \left\{ \begin{array}{c} L \\ D \\ M_\alpha \end{array} \right\}$$

The sectional loads L, D, and M_α are functions of the actual blade deformations u, v, v' etc. and may be written as

$$\left\{ \begin{array}{c} L \\ D \\ M_\alpha \end{array} \right\} = -\mathbf{m}\ddot{\mathbf{x}} - \mathbf{c}\dot{\mathbf{x}} - \mathbf{kx} + \mathbf{f}$$

where $\mathbf{m}, \mathbf{c}$, and $\mathbf{k}$ are matrices of the coefficients of the linear terms in $\{L\ D\ M_\alpha\}^T$ and $\mathbf{f}$ contains the nonlinear terms. The virtual work then becomes

$$\begin{aligned} \delta W &= \int_{\text{element}} \delta\mathbf{q}^T\mathbf{H}^T(-\mathbf{m}\ddot{\mathbf{x}} - \mathbf{c}\dot{\mathbf{x}} - \mathbf{kx} + \mathbf{f}) \\ &= \int_{\text{element}} \delta\mathbf{q}^T\mathbf{H}^T(-\mathbf{mH}\ddot{\mathbf{q}} - \mathbf{cH}\dot{\mathbf{q}} - \mathbf{kHq} + \mathbf{f}) \end{aligned}$$

leading to the aerodynamic contributions to the elemental mass, stiffness, and damping matrices:

$$\mathbf{M}_{\text{aero}} = \int_{\text{element}} \mathbf{H}^T(\xi)\mathbf{m}(\xi)\mathbf{H}(\xi)d\xi$$

$$\mathbf{C}_{\text{aero}} = \int_{\text{element}} \mathbf{H}^T(\xi)\mathbf{c}(\xi)\mathbf{H}(\xi)d\xi$$

$$\mathbf{K}_{\text{aero}} = \int_{\text{element}} \mathbf{H}^T(\xi)\mathbf{k}(\xi)\mathbf{H}(\xi)d\xi$$

$$\mathbf{F}_{\text{aero}} = \int_{\text{element}} \mathbf{H}^T(\xi)\mathbf{f}(\xi)d\xi$$

The matrices $\mathbf{m}, \mathbf{c}, \mathbf{k}$, and the vector $\mathbf{f}$ were derived in closed-form starting with the sectional loads and introducing the expressions for α, h, U_T, U_P etc. as described above. A commercially available symbolic manipulation software[21] was used allowing consistent application of an ordering scheme on an element by element basis. The integrals for $\mathbf{M}_{\text{aero}}, \mathbf{C}_{\text{aero}}, \mathbf{K}_{\text{aero}}$, and $\mathbf{F}_{\text{aero}}$ were evaluated via Gaussian quadrature.

For this study it was assumed that the flap itself is mass balanced and has negligible moment of inertia so that all mass couplings between flap and blade could be ignored. Also, the mass of the trailing edge flap actuator itself was assumed to be zero.

Solution procedure

The equations of motion are solved for periodic response via a finite element in time procedure[18]. Modified Hermitian shape functions were used for the time elements. These enforce velocity continuity at the junctions between elements but allow for internal displacement-only nodes. The hub and blade loads were computed with an element-by-element force summation. Blade pitch link loads were calculated as described in Reference 22. The resulting torsional deflections together with the pitch link stiffness and arm yield the axial pitch link loads. A modified wind tunnel trim procedure is used in which $\theta_0, \theta_{1\text{C}}$, and $\theta_{1\text{S}}$ are adjusted simultaneously in an incremental fashion until

i) the change in blade response from iteration to iteration as well as the blade first harmonic flapping are sufficiently small,

ii) C_T/σ is sufficiently close to the value prescribed, and,

iii) the lift deficiency functions satisfy a periodicity criterion , i.e. their values at $\psi = 0$ are sufficiently close to their values at $\psi = 2\pi$.

Comparison of Analytic Results with Experimental Data

Although the analysis in this study takes a well documented program as its starting point, considerable

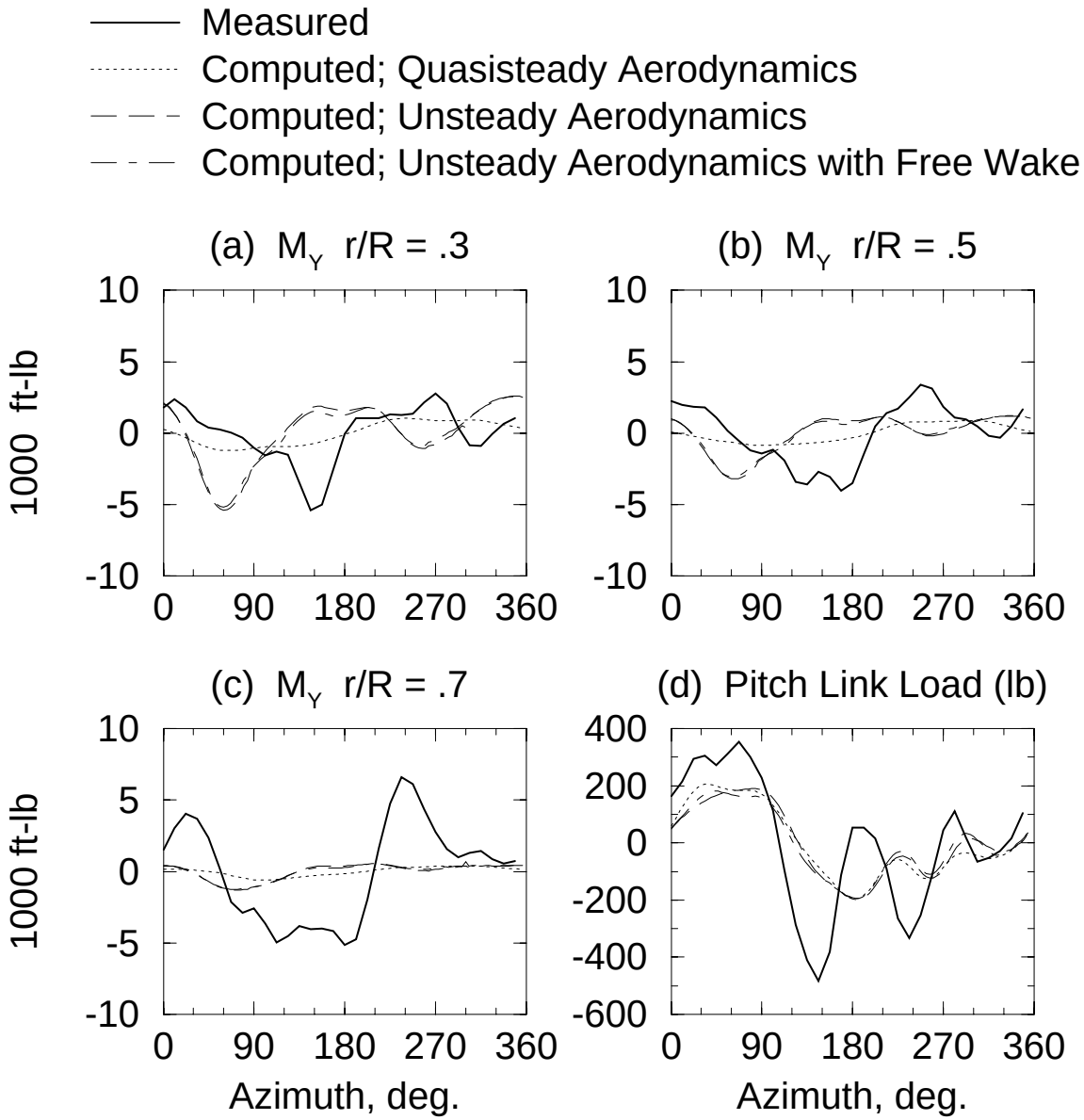

Figure 1: Comparison of predicted and measured loads. $\mu = .38$, $C_T/\sigma = .0801, \alpha_s = -5°$.

modifications were made to the aerodynamic model. Hence, before beginning the investigation, it was of primary importance to establish some confidence in the analysis. To this end, results from the present analysis were compared with available experimental data for a conventional rotor.

The experimental data set chosen for the validation study comes from a full scale wind tunnel test of a Sikorsky S-76 main rotor conducted at the NASA-Ames 40 × 80 ft. wind tunnel. Parameters measured included pitch link loads and blade bending moments at several radial stations. The loads data are documented in Reference 23. Additional discussion of this data may be found in Ref. 24.

Design data for the S-76 may be found in Refs. 25 and 26. Basic design parameters are summarized in Table 1. The rotor was modeled with five spatial elements. The Ames full-scale tests included a rectangular blade tip configuration, and these data were chosen for comparison in order to eliminate blade sweep as a potential factor in the correlation. The wind tunnel tests were performed

Table 1: Sikorsky S-76 Basic Design Data

Rotor Type	Four bladed, articulated
Radius	22 ft.
Lock Number	10.8
Solidity	.07476
Twist	7° (.3R to tip)
δ_3 coupling	17°
Flap-lag hinge offset	.038R (coincident)
Analytic Model	
Spatial elements	5
Temporal elements	5-9
Modes used	.24P (Lag), 1.03P (Flap), 2.7P (2nd Flap), 4.4P (1st Edgewise), 4.6P (3rd Flap), 5.7P (1st Torsion)

with a large fairing around the rotor drive and instrumentation which is not modeled in the present analysis. Jepson *et al*[24] have conducted an analysis accounting for inflow perturbations at the rotor disk due to the presence of the body and concluded that the body can have a significant effect on vibratory blade and pushrod loads.

Results from the correlation study are in Figs. 1a-d. Measured and computed time histories of blade flapwise bending moment and blade pitch link load are compared at an advance ratio of .38 and a $C_T/\sigma = .0801$. The computed data reflect three levels of complexity in the aerodynamic model. To allow comparison of the vibratory components of the loads, the data have been adjusted to remove their steady component. In the case of the blade bending moments, the correlation using the quasisteady model is poor. The vibratory loads are severely underpredicted. With introduction of the unsteady aerodynamic model, the harmonic content of the blade loads at .3R and .5R are very well predicted; at .7R the correlation remains poor. It is interesting to note that the .3R and .5R flatwise bending moments show good correlation of amplitude but for an apparent 90° phase shift. Introducing the free-wake model has a small effect on vibratory amplitude for this high speed flight condition. Unlike the blade bending moments in Figs. 1a-c, the pitch link loads are only slightly affected by the choice of aerodynamic model. The harmonic content of the load appears somewhat underpredicted.

It may be expected that inclusion of a dynamic stall model may improve correlation at this fairly high advance ratio (the dynamic stall model is not yet integrated with the aerodynamic model used in this analysis). Second, the aerodynamic model in Ref. 19 is based on thin symmetric airfoil theory; adjustments to account for specific airfoil properties have not been made. For example, the lift curve slope is $2\pi/\beta$ and and the pitching moment about the quarter chord is assumed to be zero. Finally, Jepson *et al*[24] suggest that a representation of inflow distortion due to presence of the wind tunnel test body is essential for accurate prediction of blade vibratory loads. Given the approximations inherent in the present analysis, the overall correlation appears adequate for the purpose of evaluating the relative effects of the trailing edge flap.

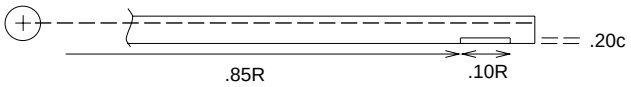

Figure 2: Baseline trailing edge flap configuration.

Results

The baseline results in this section are for the S-76 main rotor (Table 1). The baseline trailing edge flap was of 20% blade chord and extended from 85-95% blade radius (Fig. 2). The following results for the trailing edge flap rotor are calculated for wind tunnel trim at a high speed flight condition ($\mu = .38$) and nominal thrust level ($C_T/\sigma = .0801$). The data were calculated with the unsteady aerodynamic model. The free wake model, however, was found in the previous section to have little influence at this high speed flight condition and was not used.

Open Loop Flap Inputs

Initially, open loop characteristics of the blade with trailing edge flap were examined in order to gain insight into the behavior of the blade with trailing edge flap. Figure 3 shows results for the baseline flap configuration driven open loop with a 3/rev flap input. These figures map 4/rev fixed system inplane and vertical shears as a function of open loop 3/rev flap deflections. Flap deflections with sine and cosine components up to ±3° are considered. These inputs are of the same order of maginitude as those considered in Ref. 16. In Figs. 3c vertical 4/rev shears are considerably improved with a combination of zero

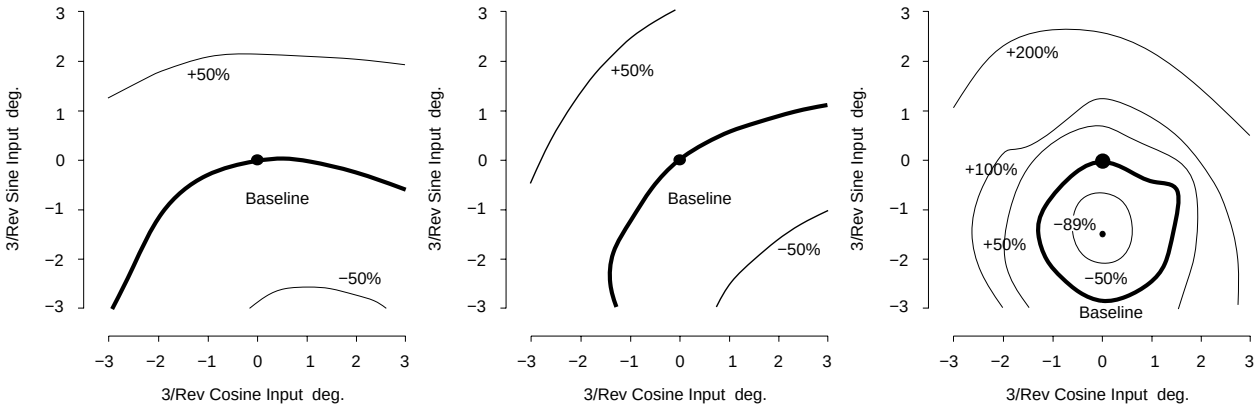

(a) 4/rev Longitudinal Shear

(b) 4/rev Lateral Shear

(c) 4/rev Vertical Shear

Figure 3: 4/rev fixed system shears with 3/rev open loop trailing edge flap input. Values shown are changes in vibratory amplitude relative to baseline (zero flap motion). $\mu = .38$, $C_T/\sigma = .0801, \alpha_s = -5°, c_f = .20$.

cosine and -1 to $-3°$ sine 3/rev inputs. Using $0°$ cosine/$-1.5°$ sine, a reduction of nearly 80% was predicted. For the inplane shears in Figs. 3b-c, the potential reduction is not as great. Also, the optimum control input for the inplane shears is somewhat different than that for the vertical shears. Nevertheless, it is clear that there are open loop inputs which will simultaneously reduce vertical and lateral shears. The results show that improper phasing of the trailing edge flap input will result in a severe vibration penalty.

The effect of the trailing edge flap input on the response of the individual blade modes may be seen in Fig. 4. The figure presents time histories of the nondimensional modal amplitude for the baseline and $0°/-1.5°$ cases discussed above. Most noticeable are the changes in the response of the third flatwise mode and the first torsion mode. A change in the 3/rev response of the third flatwise mode is observed, although not necessarily a reduction in amplitude. For reference the mode shape of the third flatwise mode is shown in Fig. 5. The trailing edge flap is located just outboard of the outer node of the flap deflection. Open loop inputs introduce a 3/rev torsional response not readily observed in the baseline case. Note it is possible for a change in 3/rev torsional response to affect the 4/rev fixed and rotating system loads. In addition, a slight reduction in the vibratory component of the amplitude of the first edgewise mode may be observed.

In Fig. 6, the harmonics of the rotating system blade root shears are shown for the baseline and $0°/-1.5°$ cases. This figure confirms that the reduction in fixed system 4/rev vertical shears observed in Fig. 3 are associated with a large reduction in rotating system 4/rev vertical shear. The improvement in fixed system 4/rev inplane shear is due to reduced 3/rev chordwise shear (F_Y). Although the fixed system results presented here are for hub shears only, the reduction in 3 and 5/rev rotating system vertical shears in Fig. 6 implies reduced 4/rev hub moments in the fixed system.

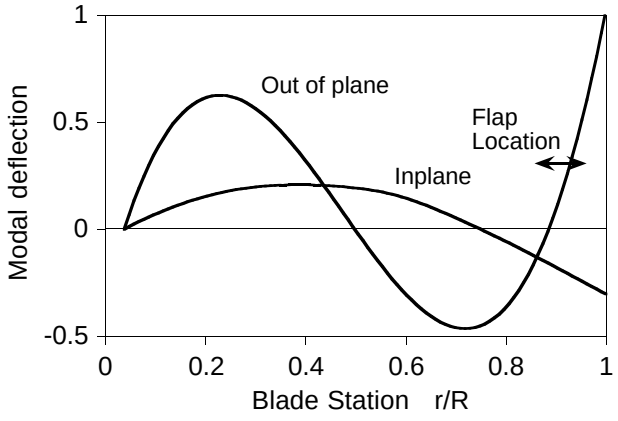

Figure 5: Mode shape of third flatwise mode (4.7/rev.)

Results for 4/rev open loop inputs are shown in Fig. 7 and 8. The 4/rev fixed system loads are more sensitive to flap inputs than those observed in the 3/rev open loop case (Fig. 3) but otherwise the results are quite similar. The optimum flap input for 4/rev vertical shear occurs around = $1°$ cosine/$.5°$ sine; here a reduction of around 90% was observed.

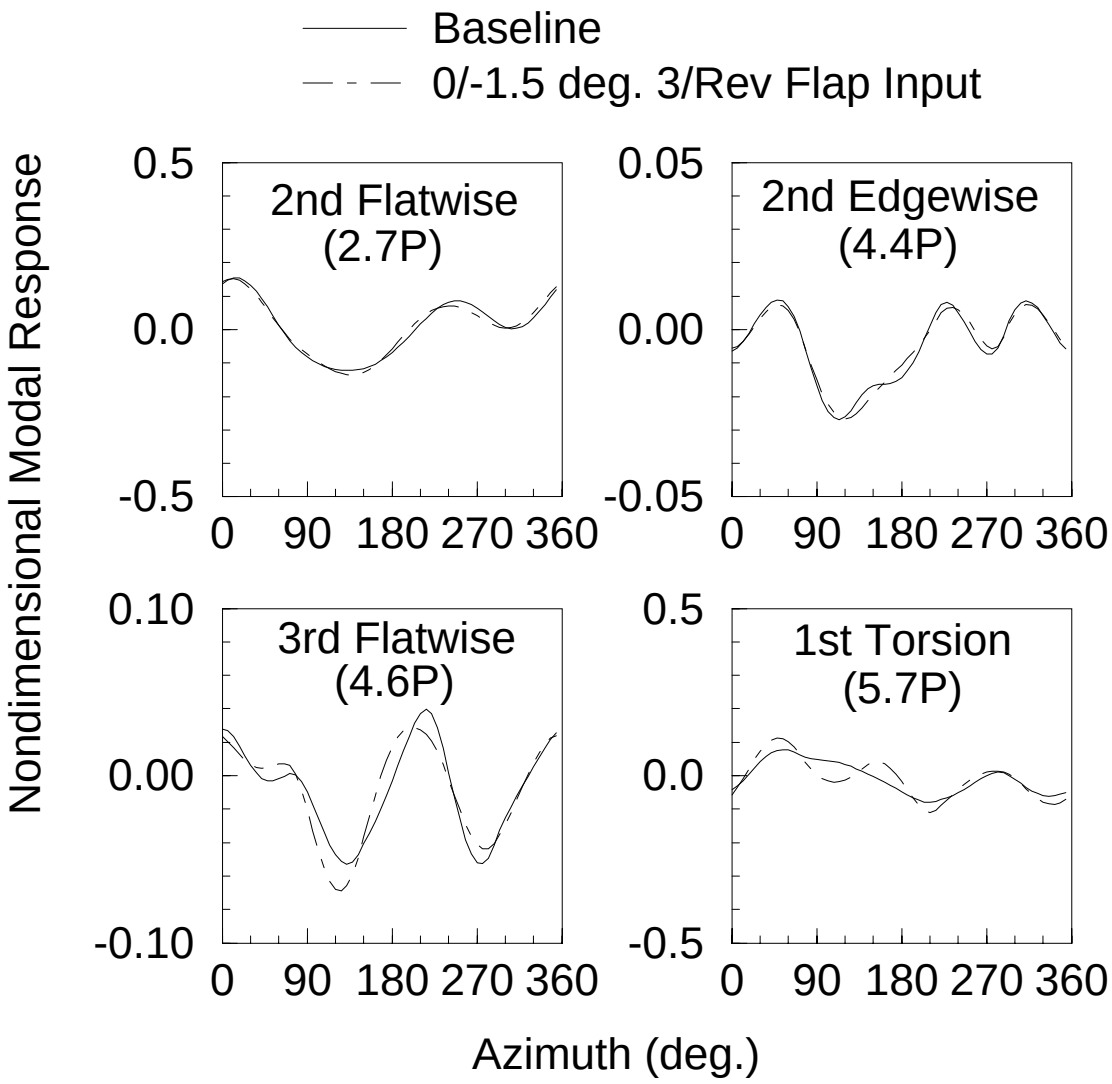

Figure 4: Time histories of modal response with and without 3/rev open loop flap inputs. $\mu = .38, C_T/\sigma = .0801, \alpha_s = -5°, c_f = .20$.

As was the case with the 3/rev open loop inputs, less effect is seen in the lateral inplane data. Fig. 8 shows the harmonic content of the rotating system blade root shear for the 4/rev open loop case. Again, the reduction in 4/rev fixed system vertical shear is a result of a large reduction in 4/rev rotating system vertical shear. The reduction in fixed system inplane shear is, as with the 3/rev input case, associated with reduced 3 and 5/rev chordwise shear (F_Y) and and 3/rev radial shear (F_X). Note that with both the 3/rev open loop inputs (Fig. 6) and the 4/rev case the combination of inputs shown for comparison optimizes the fixed system vertical 4/rev shear. A combination of inputs chosen based on fixed system inplane loads would yield reduced loads for all harmonics of the rotating system inplane loads.

Of interest is the comparison between the present results and the servo flap results in Reference 16. In this work significant vibration reductions were predicted for a servo flap controlled through a self adjusting HHC algorithm. Vibration reductions of 99% were observed upon introduction of the servo flap system. In the present investigation, reductions nearly as great are observed even in the simple open-loop case. Moreover, a comparison shows that the optimum flap deflections in the present study are no

greater than those in Ref. 16. This is, in a sense, unexpected, as the flaps in the present study are plain flaps of smaller chord than those studied in Ref. 16. However, they are also located further outboard on the blade (centered at $r/R = .90$) and are therefore more effective in bringing about blade twist than the servo flaps in Ref. 16 (centered at $r/R = .75$). Also, in Ref. 16, the flap-induced forces and moments were reduced by a substantial factor to account for effects of the gap between the trailing edge of the blade and the leading edge of the flap. In the present analysis, the plain flap is assumed to be internally sealed and thus not subject to gap effects. Finally, plain flaps are themselves capable of generating significant pitching moments and inducing blade twist. Fig. 4 shows clearly the 3/rev torsional response due to the 3/rev plain flap input.

In order to further investigate the role of vibratory blade twist on flap effectiveness, the 4/rev open loop study was repeated with the blade torsional stiffness reduced by 50%, resulting in a torsional frequency $\nu_\theta = 4.1$P (approximately $1/\sqrt{2}$ of its baseline value). The results are in Figs. 9 and 10. The fixed system 4/rev levels in Fig. 9 are quite similar to the baseline stiffness case in Fig. 7. The optimum 4/rev input is of slightly higher amplitude than in the baseline case, and is shifted in phase by nearly 90 degrees. The predicted improvements in vibration, however, are not as great. In Ref. 17, the servo flap centered at 85% blade radius also shows degraded vibration reduction effectiveness as the blade torsional natural frequency is decreased from around 5/rev to 4.3/rev. Figure 10 shows the modal response for the $\nu_\theta = 4.1$P blade with the optimum $+1.5°/-1.5°$ 4/rev input. The large increase in blade torsional response as compared with the baseline blade is expected due to the proximity of the excitation frequency to the torsional natural frequency. The other modes (second flap, third flap, and first edgewise) appear to be relatively unaffected by the flap input. It appears that vibration reductions with the plain trailing edge flap are more closely associated with changes in blade torsional response than with changes in flatwise or edgewise bending.

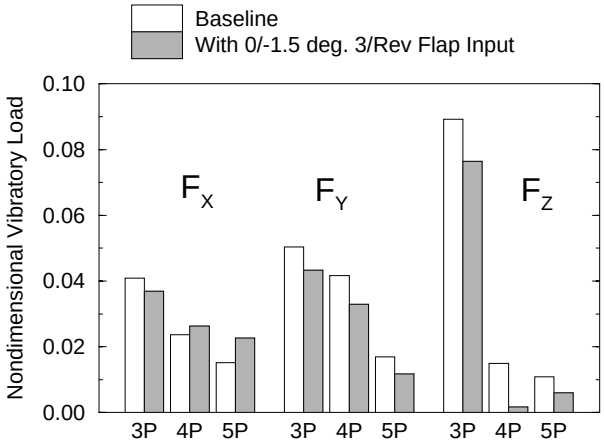

Figure 6: Harmonics of rotating system blade root shears with and without 3/rev open loop flap inputs. $\mu = .38, C_T/\sigma = .0801, \alpha_s = -5°, c_f = .20$.

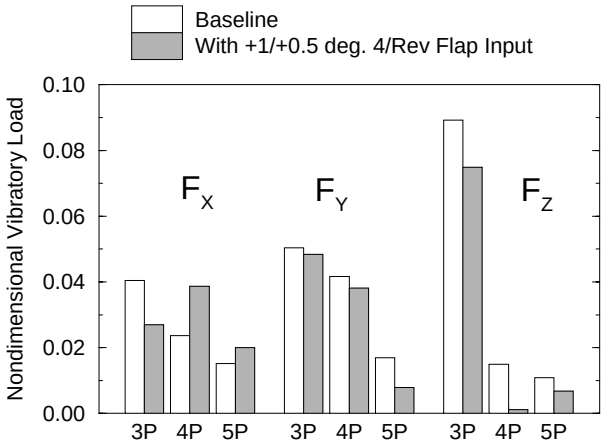

Figure 8: Harmonics of rotating system blade root shears with and without 4/rev open loop flap inputs. $\mu = .38, C_T/\sigma = .0801, \alpha_s = -5°, c_f = .20$.

Summary and Conclusions

1. A comprehensive rotorcraft dynamic analysis has been modified to model main rotor blades with plain trailing edge flaps. An unsteady aerodynamic model for a flapped airfoil has been implemented.

2. Results from the analysis were compared with previously published experimental rotor loads data for a conventional four bladed articulated main rotor. Several analytical refinements were identified which may improve the correlation.

3. Significant reductions in vibratory loads may be achieved with the flap being driven at a single frequency. Up to a 98% reduction in hub vertical 4/rev loads may be achieved with flap control inputs at 4/rev. Also, 3/rev flap inputs were also equally effective in reducing 4/rev hub loads. The gains seen in the fixed system vertical shears were larger than those predicted for the inplane shears.

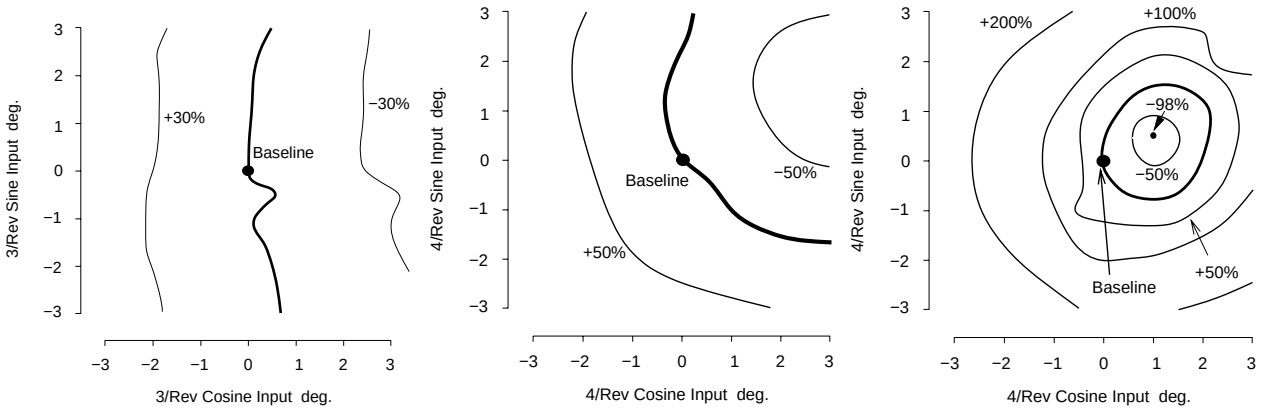

(a) 4/rev Longitudinal Shear

(b) 4/rev Lateral Shear

(c) 4/rev Vertical Shear

Figure 7: 4/rev fixed system shears with 4/rev open loop trailing edge flap input. Values shown are changes in vibratory amplitude relative to baseline (zero flap motion). $\mu = .38$, $C_T/\sigma = .0801, \alpha_s = -5°, c_f = .20$.

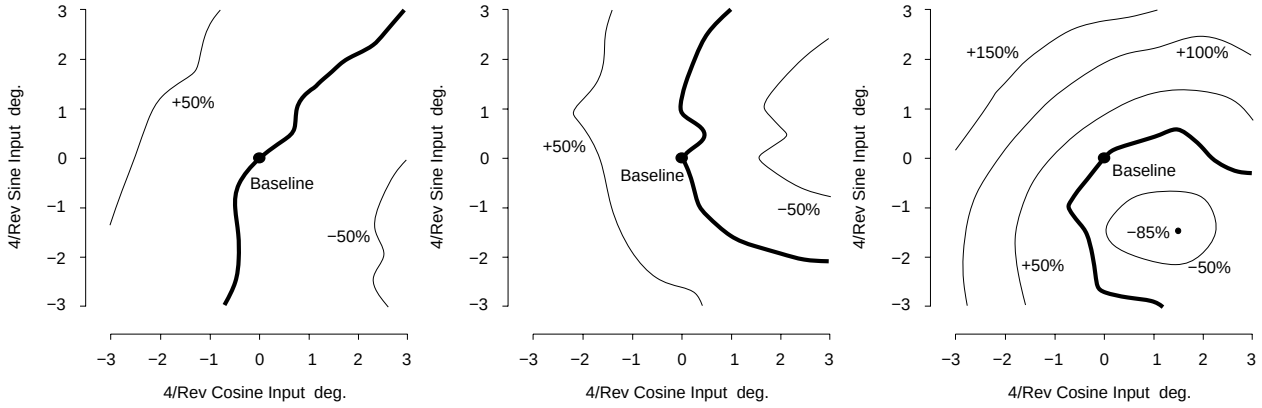

(a) 4/rev Longitudinal Shear

(b) 4/rev Lateral Shear

(c) 4/rev Vertical Shear

Figure 9: 4/rev fixed system shears with 4/rev open loop trailing edge flap input and reduced torsional stiffness ($\nu_\theta = 4.1/rev$). Values shown are changes in vibratory amplitude relative to baseline (zero flap motion). $\mu = .38$, $C_T/\sigma = .0801, \alpha_s = -5°, c_f = .20$.

4. The plain flap is intended primarily as a device for changing blade lift characteristics. Despite this, the vibration reductions predicted for the plain flap are associated with considerable changes in blade torsional response as well as flatwise and edgewise motion.

5. The vibration reduction effectiveness of the plain flap decreased when the blade torsional stiffness was reduced from its baseline value of 5.7P to 4.1P. Nevetheless, an approximately 85% reduction in fixed system 4/rev vertical shears was possible.

6. Ongoing research is aimed at refining the analytic model, examination of the effects of flap design parameters, and investigation into the feasibility of a time domain feedback control law.

Acknowledgement

The authors gratefully acknowledge the support for this research work provided by the Army Research Office under the Center for Rotorcraft Education and Research contract DAAH-04-94-G-0074, Technical Monitor Dr. Tom Doligalski.

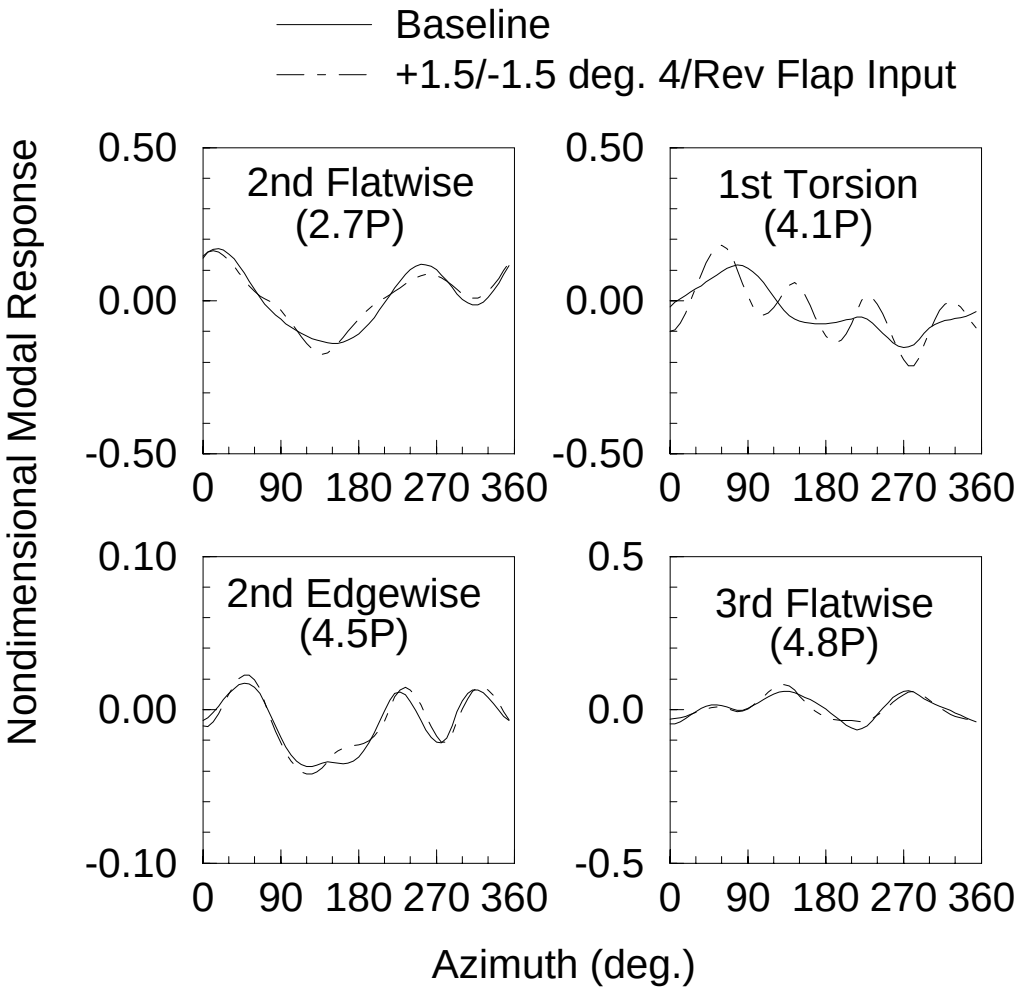

Figure 10: Time histories of modal response for reduced torsional stiffness rotor with and without 4/rev open loop flap inputs. $\mu = .38, C_T/\sigma = .0801, \alpha_s = -5°, c_f = .20$.

References

[1] Johnson, W., "Self-Tuning Regulators for Multicyclic Control of Helicopter Vibration," NASA Technical Paper 1996, March 1982.

[2] McCloud III, J. L., "Multicyclic Jet-Flap Control for Alleviation of Helicopter Blade Stresses and Fuselage Vibration," Presented at the AHS/NASA-Ames Specialists' Meeting on Rotorcraft Dynamics; NASA SP-352, 1974.

[3] Kretz, M., Aubrun, J.-N., and Larche, M., "Wind Tunnel Tests of the Dorand DH 2011 Jet Flap Rotor," NASA CR-114693, 1973.

[4] Lorber, P. and Carson, R. G., "The Aerodynamics of an Oscillating Jet Flap," *Journal of the American Helicopter Society*, Vol. 34, (2):24–32, April 1989.

[5] Lemnios, A. Z. and Dunn, F. K., "Theoretical Study of Multicyclic Control of a Controllable Twist Rotor," NASA CR-151959, Moffett Field, California.

[6] Straub, F. K. and Robinson, L. H., "Dynamics of a Rotor with Nonharmonic Control," Proceedings of the 49th Annual Forum of the American Helicopter Society, St. Louis, Missouri, May 19-21, 1993.

[7] Ben-Zeev, O. and Chopra, I., "Development of an Improved Helicopter Rotor Model Employing Smart Trailing-Edge Flaps for Vibration Suppression," Presented at the SPIE North American Conference on Smart Structures and Materials, Feb. 27-Mar. 3, 1995.

[8] Chen, P. and Chopra, I., "Induced Strain Actuation of Composite Beams and Rotor Blades with Embedded Piezoceramic Elements," Presented at the SPIE North American Conference on Smart Structures and Materials, Orlando, Florida, 1994.

[9] Ham, N. D., "Helicopter Individual-Blade-Control and its Applications," Presented at the Thirty-Ninth Annual Forum of the American Helicopter Society, St. Louis, MO, May 1983.

[10] Robinson, L. and Friedmann, P. P., "Analytic Simulation of Higher Harmonic Control Using a New Aeroelastic Model," Proceedings of the 30th Structures, Structural Dynamics and Materials Conference, Mobile, Alabama, AIAA Paper 89-1321, 1989.

[11] Spangler, R. L. and Hall, S. R., "Piezoelectric Actuators for Helicopter Rotor Control," Proceedings of the 31st AIAA Structures, Structural Dynamics, and Materials Conference. Paper AIAA-90-1076-CP, 1990.

[12] Samak, D. K. and Chopra, I., "A Feasibility Study to build a Smart Rotor: Trailing Edge Flap Actuation," Proceedings of the SPIE Conference on Smart Structures and Intelligent Systems, Albuquerque, NM, 1993.

[13] Fenn, R. C., Downer, J. R., Bushko, D. A., Gondhalekar, V., and Ham, N. D., "Terfenol-D Driven Flaps for Helicopter Vibration Reduction," Proceedings of the SPIE Conference on Smart Structures and Intelligent Systems, Albuquerque, NM, 1993.

[14] Walz, C. and Chopra, I., "Design and Testing of a Helicopter Rotor Model with Smart Trailing Edge Flaps," AIAA-94-1767-CP, Presented at the 35th Structures, Structural Dynamics and Materials Conference, Adaptive Structures Forum, April 1994.

[15] Millott, T. A. and Friedmann, P. P., "Vibration Reduction in Helicopter Rotors Using an Active Control Surface Located on the Blade," Proc. 33rd AIAA/ASME/ASCE/AHS Structures, Structural Dynamics and Materials Conference, AIAA paper 92-2451, Dallas, Texas, April 1992.

[16] Millott, T. A. and Friedmann, P. P. "The Practical Implementation of an Actively Controlled Flap to Reduce Vibrations in Helicopter Rotors,". In *Proceedings of the 49th Annual Forum of the American Helicopter Society*, pages 1079–1092, St. Louis, May 1993.

[17] Millott, T. A. and Friedmann, P. P., "Vibration Reduction in Hingeless Rotors Using an Actively Controlled Trailing Edge Flap: Implementation and Time Domain Simulation," AIAA-94-1306-CP, Presented at the 35th Structures, Structural Dynamics and Materials Conference, Adaptive Structures Forum, April 1994.

[18] Bir, G., Chopra, I., et al., "University of Maryland Advanced Rotor Code (UMARC) Theory Manual," UM-AERO 94-18, University of Maryland, College Park, Maryland, July 1994.

[19] Leishman, J. G., "Unsteady Lift of a Flapped Airfoil by Indicial Concepts," *Journal of Aircraft*, Vol. 31, (2):288–297, March-April 1994.

[20] Beddoes, T. S., "Practical Computation of Unsteady Lift," *Vertica*, Vol. 8, (1):55–71, 1984.

[21] Wolfram, S., *Mathematica: a system for doing mathematics by computer*, Addison-Wesley, Redwood City, California, 1991.

[22] Milgram, J. H. and Chopra, I., "Dynamically Tuned Blade Pitch Links for Vibration Reduction," Presented at the 50th Annual Forum of the American Helicopter Society, Washington, DC, May 1994.

[23] Johnson, W., "Performance and Loads Data from a Wind Tunnel Test of a Full-Scale Rotor with Four Blade Tip Planforms," NASA TM-81229; USAAVRADCOM TR 80-A-9, 1980.

[24] Jepson, D., Moffitt, R., Hilzinger, K., and Bissell, J., "Analysis and Correlation of Test Data From an Advanced Technology Rotor System," NASA-CR 3714, August 1983.

[25] Niebanck, C. and Girvan, W. "Sikorsky S-76 Analysis, Design, and Development for Successful Dynamic Characteristics,". In *Proceedings of the 34th Annual Forum.* American Helicopter Society, May 1978.

[26] Kottapalli, S. and Leyland, J., "Analysis of Open Loop Higher Harmonic Control at High Airspeeds on a Modern Four-Bladed Articulated Rotor," NASA TM 103876, August 1991.